molbank

MDPI

Short Note

(3-(4-Chlorophenyl)-4,5-dihydroisoxazol-5-yl)methyl Benzenesulfonate

Loubna Mokhi [1], Karim Chkirate [2], Xiaodong Zhang [3], Mohsine Driowya [1,4] and Khalid Bougrin [1,5,*]

[1] Equipe de Chimie des Plantes et de Synthèse Organique et Bioorganique, URAC 23, Faculty of Science, B.P. 1014, Geophysics, Natural Patrimony and Green Chemistry (GEOPAC) Research Center, Mohammed V University in Rabat, Rabat 10010, Morocco; loubna.mokhi@um5r.ac.ma (L.M.); m.driowya@usms.ma (M.D.)
[2] Laboratory of Heterocyclic Organic Chemistry, URAC 21, Pharmacochemistry Competence Center, Av. Ibn Battouta, B.P. 1014, Faculty of Sciences, Mohammed V University in Rabat, Rabat 10010, Morocco; k.chkirate@um5r.ac.ma
[3] Department of Chemistry, Tulane University, New Orleans, LA 70118, USA; xzhang2@tulane.edu
[4] Higher School of Technology, Sultan Moulay Slimane University, B.P. 170, Khenifra 54006, Morocco
[5] Chemical & Biochemical Sciences Green-Process Engineering (CBS), Mohammed VI Polytechnic University, Lot 660, Hay Moulay Rachid, Ben Guerir 43150, Morocco
* Correspondence: k.bougrin@um5r.ac.ma

Abstract: A novel single crystal of (3-(4-chlorophenyl)-4,5-dihydroisoxazol-5-yl)methyl benzenesulfonate has been synthetized via a one-pot sequential strategy under sonication. The single crystal has been investigated using X-ray diffraction analysis. Hydrogen bonding between C–H···O and C–H···N produces a layer structure in the crystal. According to a Hirshfeld surface analysis, interactions H···H (28.9%), H···O/O···H (26.7%) and H···C/C···H (15.8%) make the largest contributions to crystal packing. The optimized structure and the solid-state structure that was obtained through experiments are compared using density functional theory at the B3LYP/6-311 G + (d,p) level. The computed energy difference between the lowest unoccupied molecular orbital (LUMO) and highest occupied molecular orbital (HOMO) is 4.6548 eV.

Keywords: green strategy; one-pot reaction; isoxazoline sulfonate; ultrasound cavitation; X-ray analysis; hydrogen bond; Hirshfeld surface; DFT

Citation: Mokhi, L.; Chkirate, K.; Zhang, X.; Driowya, M.; Bougrin, K. (3-(4-Chlorophenyl)-4,5-dihydroisoxazol-5-yl)methyl Benzenesulfonate. *Molbank* **2023**, *2023*, M1732. https://doi.org/10.3390/M1732

Academic Editors: Antonio Salomone and Serena Perrone

Received: 30 August 2023
Revised: 14 September 2023
Accepted: 18 September 2023
Published: 22 September 2023

1. Introduction

Compounds bearing an isoxazoline moiety are considered a significant class of nitrogen and oxygen atom-containing heterocyclic products, attracting attention from organic and medicinal chemists due to their large spectrum of biological properties such as antibacterial [1,2], antimicrobial [3], anti-inflammatory [4], anticancer [5,6], antidiabetic [7] and anti-Alzheimer effects [8]. Moreover, isoxazoline derivatives are also known by their agrochemical properties as herbicidal [9], insecticidal [10–12] and acaricidal agents [13]. On the other hand, sulfonic esters are clearly identified for their crucial role in the synthesis of organic compounds and have shown interesting pharmacological properties in the past decade [14–16]. Accordingly, the synthesis of molecules containing both isoxazoline and sulfonate ester scaffolds provide easy access to a range of well-defined bioactive compounds for complete chemical, biochemical and pharmacological research [17,18]. To this end, several methods have been reported for the preparation of isoxazoline systems [19,20]. However, 1,3-dipolar cycloaddition which involves alkene as a dipolarophile and nitrile oxide as a dipole remains as one the most attractive route to prepare this aza-heterocycle [21]. As for the sulfonate ester synthesis, the most common protocol for its preparation is the reaction of sulfonyl chlorides with alcohols using a base [22]. In this study, we described the preparation and structural determination of a new isoxazoline-linked sulfonate compound utilizing an efficient and green protocol in water under ultrasound cavitation, which

emerges as a suitable alternative to previously reported methods for organic synthesis laboratories [23,24].

In addition to evaluating a molecule's activity, theoretical calculations provide valuable knowledge on a variety of the molecule's characteristics [25]. With the development of technology, the calculation of results has become more precise and faster [25]. Considering the variety of uses mentioned above, the title compound [3-(4-chlorophenyl)-4,5-dihydroisoxazol-5-yl]methyl benzenesulfonate was prepared and identified spectroscopically. The three-dimensional structure was resolved by single-crystal X-ray diffraction investigations. To determine the compound's optimal molecular structure characteristics, HOMO-LUMO energies, thermodynamic parameters, Hirshfeld surface analysis and density functional theory (DFT) computations were used to study the intermolecular interactions and hydrogen bonds. In this study, the chemical properties of the molecules were investigated employing a 6-311 + g(d,p) basis set and B3LYP techniques with Gaussian calculations.

2. Results

2.1. Synthesis

Inspired by our previous works [26,27], the one-pot synthesis of our product (**5**) started with the sulfonylation of equimolar equivalents of allylic alcohol (**1**) and benzene sulfonyl chloride (**2**) in water with NaOH as a base at 25 °C under sonication to produce the corresponding dipolarophile (**3**) in situ. Subsequently, in the second step, the alkene sulfonate (**3**) reacted with p-chlorobenzaldoxime (**4**) via 1,3-dipolar cycloaddition using NaCl as a precatalyst generated from the first step and oxone as a terminal oxidant to successfully generate the expected (3-(4-chlorophenyl)-4,5-dihydroisoxazol-5-yl)methyl benzenesulfonate (**5**) as white crystals at a 85% yield (Scheme 1).

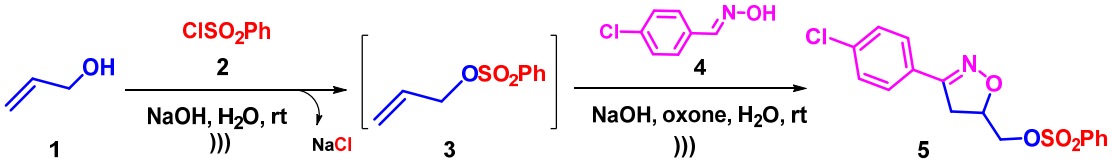

Scheme 1. One-pot synthesis of compound **5**.

The structure of isoxazoline sulfonate (**5**) was fully characterized by FT-IR, ^{1}H NMR, ^{13}C NMR and ESI^{+}-MS spectroscopies, and confirmed by single-crystal X-ray diffraction (See Figures S1–S4 in Supplementary Materials (SM) Section). As illustrated in Figure 1, the ^{1}H NMR spectrum of (**5**) showed two doublets of doublets at 3.47 and 3.12 ppm corresponding to the two protons of the CH_2-isoxazolinic as well as two doublets of doublets at 4.14 and 4.19 ppm for the O-CH_2 protons. Furthermore, we detected the presence of a multiplet centered at 4.92 ppm illustrating the H-isoxazolinic proton. Then, the region between 7.47 and 7.88 ppm showed the signals of the different aromatic protons. The ^{13}C NMR spectrum exhibited three blinded signals at 36.6, 71.6 and 78.5 ppm, corresponding to CH_2-isoxazoline, O-CH_2 and CH-isoxazoline and signals at 156.3, 135.5, 135.3, 135.0, 130.3 (2C), 129.4 (2C), 128.9 (2C), 128.3 and 128.2 (2C), attributed to all the aromatic carbons.

2.2. X-ray Analysis

X-ray intensity data were collected at 150 (2) K. Using APEX4 [28], the structure was solved via Intrinsic Phasing in the SHELXT [29] structure solution program and refined using the Least Squares minimization in the SHELXL [30] refinement package. With one molecule in the asymmetric unit, [3-(4-chlorophenyl)-4,5-dihydroisoxazol-5-yl]methyl benzenesulfonate crystallizes in the orthorhombic space group Pbca (Figure 2).

The molecules are linked by a small C–H···O contact (Figure S5, see SM) and by short C–H···N contacts to form a long chain along the a-axis (Figure S6, see SM). The molecules are linked in crystallographic symmetry in a unit cell by eight molecules forming four pairs

by connection through short C–H···O contacts (represented by blue dotted lines). Each pair will form a long chain along the a-axis through the C–H···N interactions (not shown). The four long chains interact with each other through C–H···π (ring) and C–O···π (ring) interactions, which are represented by black dotted lines (with centroids shown as of pink spheres) (Figure S7 and Table S1, see SM).

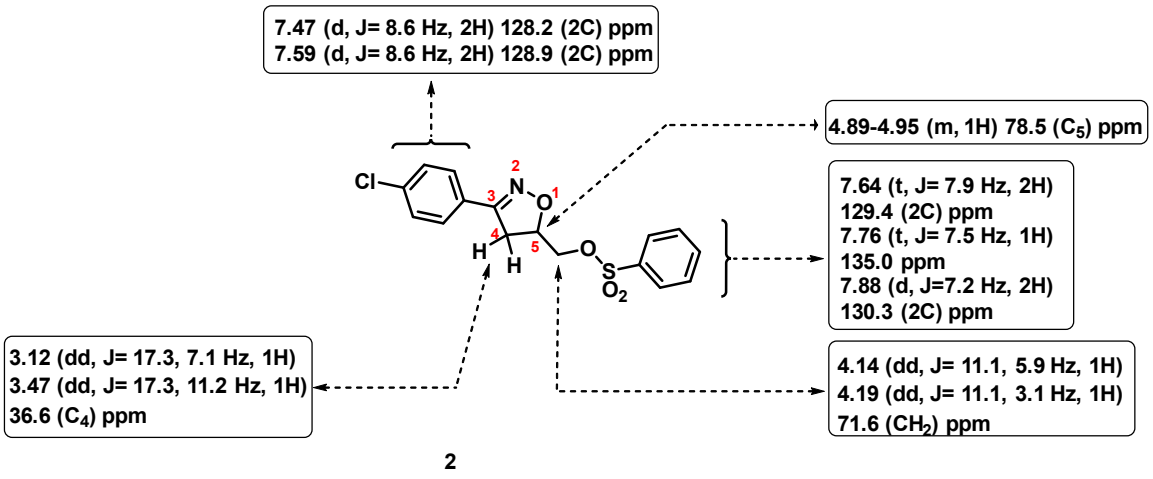

Figure 1. Characteristic ^{1}H, ^{13}C NMR of compound (**5**).

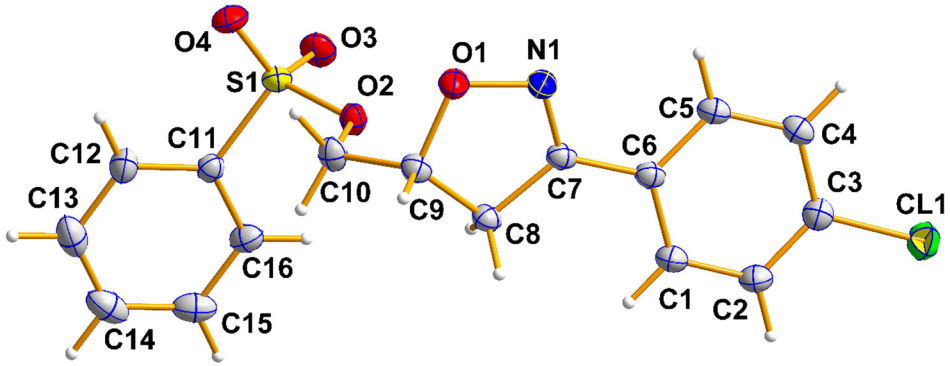

Figure 2. The title molecule with labeling scheme and 50% probability ellipsoids.

These molecules form four pairs through connections by C–H···O short contacts (depicted as blue dashed lines). Each pair will form a long chain along the a-axis through C–H···N interactions (not shown). The four long chains interact with each other through C–H···π (ring) and C–O···π (ring) interactions, which are depicted as black dashed lines (with centroids displayed as pink spheres).

Crystal Explorer 17.5 [31–33] was used to conduct a Hirshfeld surface (HS) analysis in order to see how [3-(4-chlorophenyl)-4,5-dihydroisoxazol-5-yl]methyl benzenesulfonate interacts with other molecules in the crystal. As shown in Figure 3a, the blue- and red-colored surfaces in the HS plotted over d_{norm} denote contacts with distances that are longer (distinct contact) or shorter (in close contact), respectively, whereas the white color denotes connections with distances equal to the sum of the van der Waals radii. The most important red spots and the corresponding interactions are shown in Figure S8 (See SM). The shape-index (Figure 3b) generated in the range of −1 to 1 Å shows that there are no π–π interactions, normally indicated by adjacent blue and red triangles. The sites of intimate intermolecular contacts in the compound are clearly visible in the potential electrostatic calculated utilizing the STO-3G basis, which are mapped on the Hirshfeld surface throughout the range of 0.05 a.u. and set at the Hartree–Fock level of theory (Figure 3c). Positive potential electrostatic (blue zone) over the surface denotes hydrogen-

donor potential, whereas negative electrostatic potential (red region) denotes hydrogen-bond acceptors.

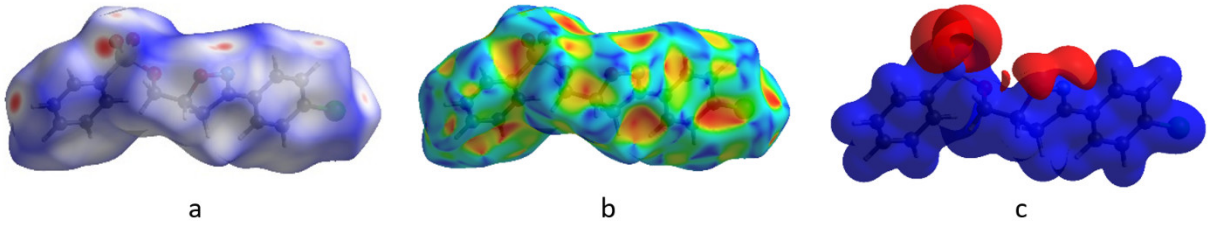

Figure 3. View of the Hirshfeld surface of [3-(4-chlorophenyl)-4,5-dihydroisoxazol-5-yl]methyl benzenesulfonate mapped (**a**) over dnorm in the range -0.2185 to 1.3206 a.u., (**b**) over shape-index map. (**c**) Electrostatic potential energy in the range −0.05 to 0.05 a.u. measured using the STO-3 G basis set at the theoretical level of Hartree–Fock.

Figure S8 (See SM) depicts the existence of multiple brilliant red spots on the three-dimensional d_{norm} surfaces of the crystal structure, which are hydrogen bonding interactions.

Figure S9a (See SM) displays the entire two-dimensional fingerprint pattern [34], while those divided into H···O/O···H, H···H, H···C/C···H, H···Cl/Cl···H, H···N/N···H, C···C, Cl···O/O···Cl and O···C/C···O contacts are illustrated in Figure S9b–i (See SM), respectively, along with their relative contributions to the Hirshfeld surface (HS). Given the high hydrogen content of the molecule and its significant contribution of 28.9% to the total crystal packing, the most significant interaction is HH, which is depicted in Figure S9b as widely scattered points of high density with a tip at $d_e = d_i = 1.28$ Å. The tips of the pair of distinctive wings in the fingerprint plot demarcated into H···O/O···H interactions (26.7%), Figure S9c, are at $d_e + d_i = 2.22$ Å when O–H interactions are present. The tips of the two distributed points of spikes in Figure S9d (15.28%), the fingerprint plot demarcated into C···H/H···C, are at $d_e + d_i = 2.74$ Å. The Cl···H/H···Cl contacts, Figure S9e (12.8%), have the tips at $d_e + d_i = 2.73$ Å. The N···H/H···N connections, Figure S9f, appear as scattered dots with spikes at $d_e + d_i = 2.42$ Å and contribute to 6.3% of the HS. The C···C contacts, Figure S9g, are a pair of distributed spike points with tips at $d_e + d_i = 3.31$ Å and contribute to 6.2% of the HS. The Cl···O/O···Cl connections, Figure S9h, are a pair of scattered spike tips that emerge with a tip at de + di = 3.42 Å and contribute to 1.9% of the HS. The O···C/C···O contacts, Figure S9i, have a low point density and only contribute to 0.7% of the total points of the HS.

2.3. Theoretical Calculation Details

DFT was used to optimize the structure of [3-(4-chlorophenyl)-4,5-dihydroisoxazol-5-yl]methyl benzenesulfonate in the gas phase. The 6-311 G + (d,p) basis-set and the hybrid B3LYP method, which are built on the model of Becke [35] and take into account a combination of the exact (Hartree-Fock) and using the B3 functional DFT exchange, as well as the LYP correlation functional [36], were used to calculate the DFT. The harmonic frequencies of vibration were estimated after obtaining the converged geometry at the same theoretical level to verify that the stationary point has no imaginary frequencies. The GAUSSIAN 09 program was used to optimize the shape and analyze the harmonic vibrational frequency of [3-(4-chlorophenyl)-4,5-dihydroisoxazol-5-yl]methyl benzenesulfonate [37]. Numerous quantum chemical parameters have been discovered as a result of these studies. Each parameter describes a particular molecule's chemical characteristics [38]. Table S2 (See SM) provides an overview of the experimental and theoretical findings regarding angles and bond lengths. Table S3 (See SM) summarizes the results for the title compound, which include hardness (η), electronegativity (χ), ionization potential (I), electron affinity (A), dipole moment (μ), softness (σ) and electrophilicity (ω). The highest occupied molecular orbital (HOMO) and lowest unoccupied molecular orbital (LUMO) properties of the molecules are more significant than the others [39]. Figure S10 (See SM) depicts the electron's change in energy level from HOMO to LUMO. The figure's brown

and green areas correspond to molecular orbitals with diametrically opposed phases. The molecule's positive phase is depicted in green, and its negative phase in brown. In the plane that spans the entire [3-(4-chlorophenyl)-4,5-dihydroisoxazol-5-yl]methyl benzenesulfonate system, the LUMO and HOMO are localized. The molecule's energy band gap is 4.6548 eV [$\Delta E = E_{LUMO} - E_{HOMO}$], and the frontier molecular orbital energies, E_{LUMO} and E_{HOMO}, are −1.9053 and −6.5601 eV, respectively.

3. Experimental Section

3.1. Materials and Methods

All reactions were followed by thin-layer chromatography (precoated sheets, Silica gel 60 F254, E. Merck), and chromatograms were viewed using UV lights at 254 and 360 nm, ^{1}H and ^{13}C NMR spectra were run in dry deuterated dimethylsulfoxide (DMSO-d_6) on a JNM-ECZ 500 spectrometer at 500 MHz for ^{1}H NMR and 126 MHz for ^{13}C NMR. The samples were diluted in CH_3CN, then mass spectra (ESI^+-MS) were determined on an Agilent Technologies 1260 Infinity II LC/MSD. Melting points were measured using Köfler Bench equipment. The reactions were sonicated using a Vibra-Cell™ ultrasonic processor model 75,022 with a Titanium alloy Ti6Al-4 V probe (20 kHz, 130 W) with a 4 mm diameter tip, and used 60% of Pmax. The sonotrode was submerged into the solution in a conical bottom flask of 25 mL in order to obtain the most energy.

3.2. Preparation of Compound **5**

In a conical bottom flask, allylic alcohol (1 mmol) was introduced to a basic solution of sodium hydroxide (1 mmol) with water (15 mL) and then benzene sulfonyl chloride (1 mmol) was added dropwise. The reaction was activated by sonication for 10 min at room temperature. Subsequently, after the completion of the sulfonylation reaction as monitored by TLC, the p-chlorobenzaldoxime (1.2 mmol), oxone (2 mmol) and sodium hydroxide (1 mmol) were added to the solution mixture at the same temperature to obtain the corresponding cycloadduct after 30 min of US irradiation (with TLC monitoring). The organic layer was extracted with DCM (3 × 10 mL) and then dried over sodium sulfate, filtered and concentrated in a vacuum. Recrystallization was employed to purify the crude product in hot ethanol and provide the desired (3-(4-chlorophenyl)-4,5-dihydroisoxazol-5-yl)methyl benzenesulfonate at a high purity.

Yield 85%, Mp 121–123 °C (ethanol), TLC (cyclohexane 90%/ethylacetate 10%) Rf = 0.6; FT-IR (ATR, cm^{-1}): 1660 (C=N), 1190 (O=S=O), 906 (N–O); ^{1}H NMR (500 MHz, DMSO-d_6) δ 7.88 (d, *J* = 7.2 Hz, 2H, Har), 7.76 (t, *J* = 7.5 Hz, 1H, Har), 7.64 (t, *J* = 7.9 Hz, 2H, Har), 7.59 (d, *J* = 8.6 Hz, 2H, Har), 7.47 (d, *J* = 8.6 Hz, 2H, Har), 4.95–4.89 (m, 1H, C5H-isoxazoline), 4.19 (dd, *J* = 11.1, 3.1 Hz, 1H, O–CH), 4.14 (dd, *J* = 11.1, 5.9 Hz, 1H, O–CH), 3.47 (dd, *J* = 17.3, 11.2 Hz, 1H, C4H-isoxazoline), 3.12 (dd, *J* = 17.3, 7.1 Hz, 1H, C4H-isoxazoline). ^{13}C NMR (126 MHz, DMSO-d_6) δ 156.3, 135.5, 135.3, 135.0, 130.3 (2C), 129.4 (2C), 128.9 (2C), 128.3, 128.2 (2C), 78.5 (CH-isoxazoline), 71.6 (O–CH_2), 36.6 (CH_2-isoxazoline). MS (ESI^+): m/z = 352.3 $[M + H]^+$, 725.7 $[M + Na]^+$.

3.3. X-ray Crystal Structure Data

Table S4 (See SM) provides the data collection, crystal data and refined structural information. F2 has been improved to combat ALL reflections. The traditional R-factors based on F, were calculated with F set to zero for negative F2, and the weighted R-factor wR and goodness of fit S were based on F2. The selection of reflections for refinement was unrelated to expression at a threshold of F2 > 2 sigma (F2), which is utilized solely for computing R-factors (gt), etc. R-factors based on F2 will be statistically even larger than those based on F, which are statistically nearly twice as large. With the determined positions (C–H = 0.95 − 0.99 Å) and using contributions with isotropic displacement values 1.2–1.5 times that of the linked atoms, H-atoms connected to carbon were positioned in the correct positions.

4. Conclusions

In summary, we proposed an efficient and facile route to synthesize (3-(4-chlorophenyl)-4,5-dihydroisoxazol-5-yl)methyl benzenesulfonate **5** in water using an environmentally friendly protocol involving a one-pot strategy combined with ultrasound cavitation. The desired product (**5**) was obtained at a good yield and high purity, and its structure was determined by ^{1}H, ^{13}C NMR, ESI^{+}-MS and IR spectroscopies and confirmed by single-crystal X-ray diffraction. The Hirshfeld surface was used to elaborate on the research of intra- and intermolecular interactions, and a comparative theoretical analysis was also detailed.

Supplementary Materials: The following supporting materials, containing ^{1}H, ^{13}C NMR, mass spectra and IR spectra (Figures S1–S4) of the synthesized compound (**5**), Figures S5–S10 and Tables S1–S4 can be downloaded online [28–30,40,41].

Author Contributions: Conceptualization, approach, writing and original draft research, K.B., L.M., M.D. and K.C.; X-ray crystallography experiments and structural analyses carried out by X.Z.; Hirshfeld surface investigation and spectroscopic studies completed by K.C.; investigation, writing, review and editing, K.B. All authors have read and agreed to the published version of the manuscript.

Funding: This work received no external funding support.

Data Availability Statement: Not applicable.

Acknowledgments: This work is supported by UM5R and UM6P. The authors thank UATRS-CNRST Morocco.

Conflicts of Interest: The authors declare no conflict of interest.

References

1. Aarjane, M.; Slassi, S.; Ghaleb, A.; Tazi, B.; Amine, A. Synthesis, biological evaluation, molecular docking and in silico ADMET screening studies of novel isoxazoline derivatives from acridone. *Arab. J. Chem.* **2021**, *14*, 103057–103069. [CrossRef]
2. Kudryavtseva, T.N.; Lamanov, A.Y.; Sysoev, P.I.; Klimova, L.G. Synthesis and antibacterial activity of new acridone derivatives containing an isoxazoline fragment. *Russ. J. Gen. Chem.* **2020**, *90*, 45–49. [CrossRef]
3. Chalkha, M.; Nour, H.; Chebbac, K.; Nakkabi, A.; Bahsis, L.; Bakhouch, M.; Akhazzane, M.; Bourass, M.; Chtita, S.; Bin Jardan, A.Y.; et al. Synthesis, Characterization, DFT Mechanistic Study, Antimicrobial Activity, Molecular Modeling, and ADMET Properties of Novel Pyrazole-isoxazoline Hybrids. *ACS Omega* **2022**, *7*, 46731–46744. [CrossRef]
4. Rasool, J.U.; Sawhney, G.; Shaikh, M.; Nalli, Y.; Madishetti, S.; Ahmed, Z.; Ali, A. Site selective synthesis and anti-inflammatory evaluation of Spiro-isoxazoline stitched adducts of arteannuin B. *Bioorg. Chem.* **2021**, *117*, 105408–105417. [CrossRef]
5. Shaik, A.; Bhandare, R.R.; Palleapati, K.; Nissankararao, S.; Kancharlapalli, V.; Shaik, S. Antimicrobial, antioxidant, and anticancer activities of some novel isoxazole ring containing chalcone and dihydropyrazole derivatives. *Molecules* **2020**, *25*, 1047. [CrossRef]
6. Bernal, C.C.; Vesga, L.C.; Mendez-Sánchez, S.C.; Romero Bohórquez, A.R. Synthesis and anticancer activity of new tetrahydroquinoline hybrid derivatives tethered to isoxazoline moiety. *Med. Chem. Res.* **2020**, *29*, 675–689. [CrossRef]
7. Goyard, D.; Kónya, B.; Chajistamatiou, A.S.; Chrysina, E.D.; Leroy, J.; Balzarin, S.; Maurel, P. Glucose-derived spiro-isoxazolines are anti-hyperglycemic agents against type 2 diabetes through glycogen phosphorylase inhibition. *Eur. J. Med. Chem.* **2016**, *108*, 444–454. [CrossRef]
8. Huang, M.; Suk, D.H.; Cho, N.C.; Bhattarai, D.; Kang, S.B.; Kim, Y.; Keum, G. Synthesis and biological evaluation of isoxazoline derivatives as potent M1 muscarinic acetylcholine receptor agonists. *Bioorg. Med. Chem. Lett.* **2015**, *25*, 1546–1551. [CrossRef]
9. Yang, J.; Guan, A.; Wu, Q.; Cui, D.; Liu, C. Design, synthesis and herbicidal evaluation of novel uracil derivatives containing an isoxazoline moiety. *Pest Manag. Sci.* **2020**, *76*, 3395–3402. [CrossRef]
10. Jiang, B.; Feng, D.; Li, F.; Luo, Y.; He, S.; Dong, Y.; Hu, D. Design, Synthesis, and Insecticidal Activity of Novel Isoxazoline Compounds That Contain Meta-diamides against Fall Armyworm (*Spodoptera frugiperda*). *J. Agric. Food Chem.* **2023**, *71*, 1091–1099. [CrossRef]
11. Zhang, C.; Yuan, H.; Hu, Y.; Li, X.; Gao, Y.; Ma, Z.; Lei, P. Structural Diversity Design, Synthesis, and Insecticidal Activity Analysis of Ester-Containing Isoxazoline Derivatives Acting on the GABA Receptor. *J. Agric. Food Chem.* **2023**, *71*, 3184–3191. [CrossRef]
12. Mahmoudi, A.E.; Fegrouche, R.; Tachallait, H.; Lumaret, J.P.; Arshad, S.; Karrouchi, K.; Bougrin, K. Green Synthesis, Characterization, and Biochemical Impacts of New Bioactive Isoxazoline-sulfonamides as Potential Insecticidal Agents against the Sphodroxia Maroccana Ley. *Pest Manag. Sci.* **2023**. [CrossRef]
13. Shan, X.; Lv, M.; Wang, J.; Qin, Y.; Xu, H. Acaricidal and insecticidal efficacy of new esters derivatives of a natural coumarin osthole. *Ind. Crops Prod.* **2022**, *182*, 114855–114862. [CrossRef]
14. Krishna, P. Chemoselective synthesis of 5-Amino-7-Bromoquinolin-8-Yl Sulfonate derivatives and their antimicrobial evaluation. *Phosphorus Sulfur Silicon Relat. Elem.* **2018**, *193*, 685–690. [CrossRef]

15. Kanabar, D.; Farrales, P.; Gnanamony, M.; Almasri, J.; Abo-Ali, E.M.; Otmankel, Y.; Shaha, H.; Nguyen, D.; Menyewia, M.E.; Dukhande, V.V.; et al. Structural modification of the aryl sulfonate ester of cjoc42 for enhanced gankyrin binding and anti-cancer activity. *Bioorg. Med. Chem. Lett.* **2020**, *30*, 126889–126893. [CrossRef]
16. Xie, D.; Yang, Z.; Hu, X.; Wen, Y. Synthesis, antibacterial and insecticidal activities of novel capsaicin derivatives containing a sulfonic acid esters moiety. *Front. Chem.* **2022**, *10*, 929050–929057. [CrossRef]
17. Yu, M.; Liu, G.; Zhang, Y.; Feng, T.; Xu, M.; Xu, H. Design, synthesis and evaluation of novel isoxazolines/oxime sulfonates of 2′(2′, 6′)-(di) chloropodophyllotoxins as insecticidal agents. *Sci. Rep.* **2016**, *6*, 33062–33073. [CrossRef]
18. Kaur, K.; Kumar, V.; Sharma, A.K.; Gupta, G.K. Isoxazoline containing natural products as anticancer agents: A review. *Eur. J. Med. Chenm.* **2014**, *77*, 121–133. [CrossRef]
19. Liao, J.; Ouyang, L.; Jin, Q.; Zhang, J.; Luo, R. Recent advances in the oxime-participating synthesis of isoxazolines. *Org. Biomol. Chem.* **2020**, *18*, 4709–4716. [CrossRef]
20. Liu, Y.; Meng, J.; Li, C.; Lin, L.; Xu, Y. Progress in the Synthesis of Isoxazoline Derivatives by Cycloylation of Allyl Oxime. *Chin. J. Org. Chem.* **2020**, *40*, 2742. [CrossRef]
21. Rane, D.; Sibi, M. Recent advances in nitrile oxide cycloadditions. Synthesis of isoxazolines. *Curr. Org. Synth.* **2011**, *8*, 616–627. [CrossRef]
22. Lei, X.; Jalla, A.; Abou Shama, M.A.; Stafford, J.M.; Cao, B. Chromatography-free and eco-friendly synthesis of aryl tosylates and mesylates. *Synthesis* **2015**, *47*, 2578–2585. [CrossRef]
23. Alaoui, S.; Driowya, M.; Demange, L.; Benhida, R.; Bougrin, K. Ultrasound-assisted facile one-pot sequential synthesis of novel sulfonamide-isoxazoles using cerium (IV) ammonium nitrate (CAN) as an efficient oxidant in aqueous medium. *Ultrason. Sonochem.* **2018**, *40*, 289–297. [CrossRef] [PubMed]
24. Talha, A.; Favreau, C.; Bourgoin, M.; Robert, G.; Auberger, P.; Ammari, L.E.; Saadi, M.; Benhida, R.; Martin, A.R.; Bougrin, K. Ultrasound-assisted one-pot three-component synthesis of new isoxazolines bearing sulfonamides and their evaluation against hematological malignancies. *Ultrason. Sonochem.* **2021**, *78*, 105748–105759. [CrossRef]
25. El Mahmoudi, A.; Chkirate, K.; Tachallait, H.; Van Meervelt, L.; Bougrin, K. 2-((3-(4-Methoxyphenyl)-4,5-dihydroisoxazol-5-yl)methyl)benzo[d]isothiazol-3(2H)-one1,1-dioxide. *Molbank* **2022**, *2022*, M1488. [CrossRef]
26. El Mahmoudi, A.; Chkirate, K.; Mokhi, L.; Mague, J.T.; Bougrin, K. 2-(N-allylsulfamoyl)-N-propylbenzamide. *Molbank* **2023**, *2023*, M1678. [CrossRef]
27. Thari, F.Z.; Tachallait, H.; El Alaoui, N.E.; Talha, A.; Arshad, S.; Álvarez, E.; Karrouchi, K.; Bougrin, K. Ultrasound-assisted one-pot green synthesis of new N-substituted-5-arylidene-thiazolidine-2, 4-dione-isoxazoline derivatives using NaCl/Oxone/Na3PO4 in aqueous media. *Ultrason. Sonochem.* **2020**, *68*, 105222–105251. [CrossRef]
28. Bruker. *APEX4, SAINT & SHELXTL*; Bruker AXS LLC.: Madison, WI, USA, 2021.
29. Sheldrick, G.M. SHELXT—Integrated space-group and crystal-structure determination. *Acta Cryst. A* **2015**, *71*, 3–8. [CrossRef]
30. Sheldrick, G.M. Crystal structure refinement with SHELXL. *Acta Cryst. C* **2015**, *71*, 3–8. [CrossRef]
31. Hirshfeld, F.L. Bonded-atom fragments for describing molecular charge densities. *Theor. Chim. Acta* **1977**, *44*, 129–138. [CrossRef]
32. Spackman, M.A.; Jayatilaka, D. Hirshfeld surface analysis. *Cryst. Eng. Comm.* **2009**, *11*, 19–32. [CrossRef]
33. Turner, M.J.; McKinnon, J.J.; Wolff, S.K.; Grimwood, D.J.; Spackman, P.R.; Jayatilaka, D.; Spackman, M.A. *CrystalExplorer17*; The University of Western Australia: Perth, Australia, 2017.
34. McKinnon, J.J.; Jayatilaka, D.; Spackman, M.A. Towards quantitative analysis of intermolecular interactions with Hirshfeld surfaces. *Chem. Commun.* **2007**, 3814–3816. [CrossRef] [PubMed]
35. Becke, A.D. Density-functional thermochemistry. III. The role of exact exchange. *J. Chem. Phys.* **1993**, *98*, 5648–5652. [CrossRef]
36. Lee, C.; Yang, W.; Parr, R.G. Development of the Colle-Salvetti correlation-energy formula into a functional of the electron density. *Phys. Rev. B* **1988**, *37*, 785–789. [CrossRef] [PubMed]
37. Frisch, M.J.; Trucks, G.W.; Schlegel, H.B.; Scuseria, G.E.; Robb, M.A.; Cheeseman, J.R.; Scalmani, G.; Barone, V.; Mennucci, B.; Petersson, G.; et al. *GAUSSIAN09*, revision A.02; Gaussian Inc.: Wallingford, CT, USA, 2009.
38. Chkirate, K.; Essassi, E.M. Pyrazole and Benzimidazole Derivatives: Chelating Properties Towards Metals Ions and their Applications. *Curr. Org. Chem.* **2022**, *26*, 1735–1766. [CrossRef]
39. Faraj, I.; Oubella, A.; Chkirate, K.; Al Mamari, K.; Hökelek, T.; Mague, J.T.; El Ghayati, L.; Sebbar, N.K.; Essassi, E.M. Crystal structure, Hirshfeld surface analysis and DFT calculations of (E)-3-[1-(2-hydroxyphenylanilino)ethylidene]-6-methylpyran-2,4-dione. *Acta Cryst. E* **2022**, *78*, 864–870. [CrossRef]
40. Krause, L.; Herbst-Irmer, R.; Sheldrick, G.M.; Stalke, D. Comparison of silver and molybdenum microfocus X-ray sources for single-crystal structure determination. *J. Appl. Cryst.* **2015**, *48*, 3–10. [CrossRef]
41. Brandenburg, K.; Putz, H. *DIAMOND*; Crystal Impact GbR: Bonn, Germany, 2012.